ELSEVIER

Journal of Applied Geophysics 50 (2002) 351–373

JOURNAL OF APPLIED GEOPHYSICS

www.elsevier.com/locate/jappgeo

Gravitational attraction of solids of revolution Part 2: General expressions

Brian N. Damiata [a,b,*], Tien-Chang Lee [a]

[a] *Department of Earth Sciences, Institute of Geophysics and Planetary Physics, University of California, Riverside, CA 92521, USA*
[b] *Cotsen Institute of Archaeology, University of California, Los Angeles, CA 90095-1510, USA*

Received 30 May 2001; received in revised form 21 March 2002; accepted 2 April 2002

Abstract

A general integral expression is formulated for the gravitational attraction due to any solid of revolution based on the attraction of vertical, semi-infinite, circular, cylindrical shells. The expression accommodates solids with radial variation of density. For solids with constant density, further generalization to arbitrary orientation is made through coordinate transformation that considers both vertical and radial components of attraction. Special solutions for solids with simple geometry are listed. Practical applications are demonstrated by forward gravity modelling the effects of volcanic islands (cylindrical core bounded by an outer exponentially trending surface) and inclined finite-length cylinders. Corresponding expressions for the magnetic case are discussed in terms of using Poisson's relation.

Keywords: Gravitational attraction; Solids of revolution; Inclined finite-length cylinder

1. Introduction

This paper extends the work presented in Part 1 (Damiata and Lee, this volume) that dealt with the gravitational attraction of vertical, semi-infinite, circular cylinders and horizontal circular disks. The emphasis here is on formulating general expressions for the gravitational attraction due to any solid of revolution. These solutions, in turn, have wide application such as forward gravity modelling the effects of volcanic islands, lithospheric deflection and tunnels. Our primary motivation for these works concerns the simulated gravitational response due to hydraulic testing of groundwater aquifers. The solution to this axisymmetric problem calls for the attraction of a solid of revolution with radial variation of density. Such solution is not suited for polyhedron approximations that are presently available (e.g., Götze and Lahmeyer, 1988; Pohánka, 1988). Results of the groundwater problem will be reported in a future paper.

Several studies dealing with the gravitational attraction of solids of revolution are reported in the literature; all assume constant density. Duska (1958) derived solutions for the maximum gravitational attraction (i.e., along the vertical axis) of certain solids by using the formula for a circular lamina. Reilly (1969) derived both gravitational and magnetic expressions for a finite-length right circular cylinder based on an infinite series of Legendre polynomials. His solution was used to model the effects of seamounts (Woodward, 1970) and volcanic roots (Reilly,

* Corresponding author. Department of Earth Sciences, Institute of Geophysics and Planetary Physics, University of California, Riverside, CA 92521, USA.
E-mail address: damiata@ucrac1.ucr.edu (B.N. Damiata).

0926-9851/02/$ - see front matter
PII: S0926-9851(02)00152-0

1972) and was generalized to any solid of revolution by Woodward (1973). The latter's technique is based on numerically integrating the first and second derivatives of the potential for a circular lamina. The integration is performed over the length of the solid by using an N-point Gauss–Legendre integration scheme that requires $4N$ sums of infinite series of Legendre polynomials.

Pant and Govindarajan (1979) give a FORTRAN code to compute the gravitational attraction of solids that can be approximated by a set of circular disks. Their code requires numerical integration of Bessel and exponential functions. Bodine and Karner (1981) discussed a technique utilizing a one-dimensional Fast Fourier Transform that requires a linear array to describe the shape of the solid. Their technique is particularly useful for modelling long-wavelength bodies such as oceanic seamounts or sedimentary basins. Finally, Paul (1985) presented a scheme to approximate radial profiles based on a linear combination of values computed along the vertical axis.

In this paper, general expressions are formulated and a numerical technique is presented for calculating the gravitational attraction due to any solid of revolution with radial variation of density. The derivation is based on the attraction of vertical, semi-infinite, circular, cylindrical shells of infinitesimal thickness. For solids with constant density, further generalization to arbitrary orientation is made through coordinate transformation that considers both vertical and radial components of attraction. Practical applications are demonstrated by forward gravity modelling the effects of volcanic islands and inclined finite-length cylinders. Corresponding expressions for the magnetic case are briefly discussed in terms of using Poisson's relation.

2. Mathematical development

2.1. Attraction of a vertical, semi-infinite, circular, cylindrical shell

An expression for the vertical component of gravitational attraction of a vertical, semi-infinite, circular cylinder with radial variation of density was derived in Part 1 (Damiata and Lee, this volume, Eq. (15)). The attraction of a vertical, semi-infinite, circular, cylindrical shell of infinitesimal thickness can be obtained from this expression by superimposing two cylinders with slightly different radii, a, shrinking this difference to zero, and replacing the volume–mass density, $\rho'[r']$, with a surface-mass density, $\sigma'[r']$, such that $\sigma'[r'] = \rho'[r']\Delta a$ but remains nonzero as $\Delta a \to 0$. This operation is equivalent to taking the derivative with respect to a,

$$g_z^{\text{shell}}[r, z;\ \zeta] = \frac{\partial}{\partial a} g_z[r, z;\ \zeta]\Delta a = 4G\sigma'[r'] \frac{a}{\sqrt{(r+a)^2 + (\zeta - z)^2}} \times K[k_1] \quad (1)$$

where $K[k_1]$ is the complete elliptic integral of the first kind (Byrd and Friedman, 1954, Eq. (110.06), p. 9) with the modulus

$$k_1 = \sqrt{\frac{4ar}{(a+r)^2 + (\zeta - z)^2}}.$$

Fig. 1 depicts normalized gravitational attractions versus normalized vertical and radial distances for a cylindrical shell of infinitesimal thickness. The attractions of a spherical shell of infinitesimal thickness are also plotted for comparison. Note that a singularity occurs in Eq. (1) when both $\zeta - z = 0$ and $r = a$ because as such, $k_1 = 1$ and $K[1] = \infty$.

2.2. Technique based on vertical cylindrical shells

The vertical component of gravitational attraction due to *any* solid of revolution can be determined simply by adding the effects of semi-infinite cylindrical shells that bound the top surface and subtracting the effects of those that bound the bottom surface. The net effect for any given pair of shells is the attraction of a finite-length cylindrical shell as schematically illustrated in Fig. 2. The net result of integrating all such pairs is the attraction of the solid of revolution which is conceptually stated as

$$g_z[r, z] = \int_{\text{t}} f[r']\mathrm{d}r' - \int_{\text{b}} g[r']\mathrm{d}r' \quad (2)$$

where the subscripts "t" and "b" refer to the top and bottom surfaces of the solid, respectively, and $f[r']$ and $g[r']$ are functions with form similar to Eq. (1).

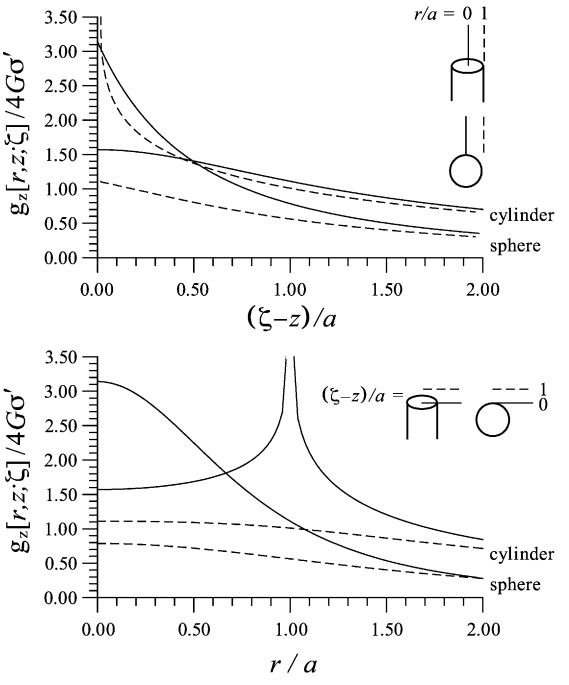

Fig. 1. Normalized gravitational attraction, $g_z[r, z; \zeta]/4G\sigma'$, of a semi-infinite cylindrical shell of infinitesimal thickness. Upper: attractions versus normalized vertical distance, $(\zeta - z)/a$, at normalized radial distances of 0 (solid line) and 1 (dashed line). Lower: attractions versus normalized radial distance, r/a, at normalized vertical distances of 0 (solid line) and 1 (dashed line). The attractions of a spherical shell of infinitesimal thickness are presented for comparison.

More specifically, for solids of revolution whose top and bottom surfaces are described by single functions (e.g., spheroid and cone), the integrals can be combined such that

$$g_z[r, z] = 4G \int_{R_1}^{R_2} \left\{ \frac{K[k_t]}{\sqrt{(r+r')^2 + (Z_t[r'] - z)^2}} - \frac{K[k_b]}{\sqrt{(r+r')^2 + (Z_b[r'] - z)^2}} \right\} \times \rho'[r'] r' \mathrm{d}r' \quad (3)$$

where R_1 and R_2 are the inner and outer radii of the solid, respectively, $Z_\upsilon[r']$ describes the vertical variation of either the top ($\upsilon =$ "t") or bottom ($\upsilon =$ "b") outer surface as a function of radial distance, and

$$k_\upsilon = \sqrt{\frac{4rr'}{(r+r')^2 + (Z_\upsilon[r'] - z)^2}}.$$

This integral can be evaluated numerically using a general or adaptive Simpson's rule for which algorithms are readily available (e.g., Press et al., 1992; Shampine and Allen, 1973). Care in numerical integration is needed, however, when the observation point lies on the surface of the solid because of the

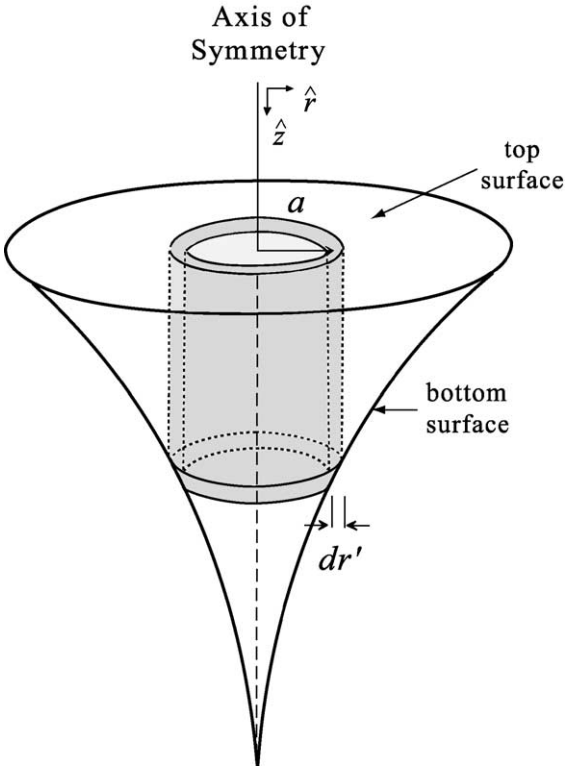

Fig. 2. Schematic diagram illustrating the technique of semi-infinite cylindrical shells to determine the gravitational attraction of a solid of revolution. The net effect of subtracting the attraction of a semi-infinite shell that bounds the bottom surface of the solid from one with the same radius that bounds the top surface is the attraction of the finite-length shell denoted by the shaded volume.

apparent singularity that occurs in the integrand even though the integral itself is finite. For this case, an analytical solution should be incorporated into the algorithm if available (e.g., see (Eqs. (A4) and (A5) in Appendix A for observation along the surface of a solid cylinder). Alternatively, the integral should be rewritten such that the singularity occurs at one of the limits and then a numerical integration scheme that does not require evaluation at the endpoints used (e.g., adaptive quadrature routine QAGS in QUADPACK sublibrary, Piessens et al., 1983; Zwillinger, 1992).

Table A1 in Appendix A lists the defining parameters for numerically evaluating the vertical component of gravitational attraction for various solids of revolution. Note that more than one integral may be needed to fully describe solids with relatively complicated surfaces. Also note that as a special case, the gravitational attraction along the rotational axis (i.e., $r=0$ in Eq. (3)) has the form

$$g_z[0,\, z] = 2\pi G \int_{R_1}^{R_2} \left\{ \frac{1}{\sqrt{r'^{\,2} + (Z_t[r'] - z)^2}} - \frac{1}{\sqrt{r'^{\,2} + (Z_b[r'] - z)^2}} \right\} \rho'[r'] r' \mathrm{d}r' \qquad (4)$$

which often can be solved explicitly for solids with simple shape and variation of density. Appendix A also contains special solutions that are provided without derivation for those solids listed in Table A1.

2.3. Technique based on horizontal circular disks

For comparison purposes, we briefly state an alternative but more cumbersome technique that can be used to calculate the gravitational attraction due to a solid of revolution. This procedure involves the "stacking" of horizontal circular disks of finite thickness as schematically illustrated in Fig. 3.

Refinement of the stacking can be achieved by integrating the solution for a disk with infinitesimal thickness as depicted in Fig. 4. The general solutions

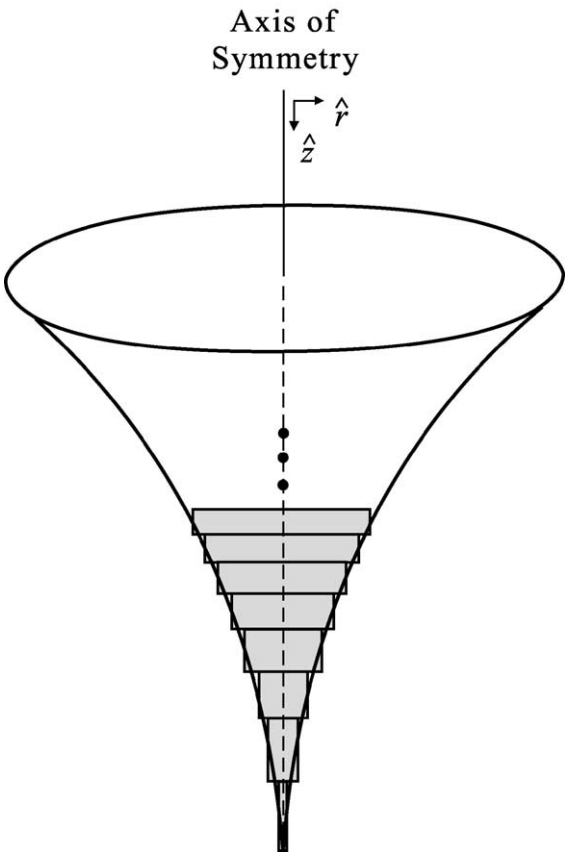

Fig. 3. Schematic diagram illustrating the technique of stacking horizontal circular disks of finite thickness to approximate the gravitational attraction of a solid of revolution.

for a thin disk with radial variation of density and constant density were derived in Part 1 (Damiata and Lee, this volume, Eqs. (45) and (48), respectively). The vertical attraction due to a solid of revolution is obtained by integrating along the axial length of the solid. As an example for the case of constant density, the desired expression for $r<a$ is

$$g_z[r,\, z]_{r<a} = 2G\rho \int_{z_t}^{z_b} \left\{ \pi - \frac{(\zeta' - z)}{\sqrt{(a[\zeta'] + r)^2 + (\zeta' - z)^2}} \times K[k_2] - \frac{\pi}{2} \Lambda_0[\phi,\, k_2] \right\} \mathrm{d}\zeta' \qquad (5)$$

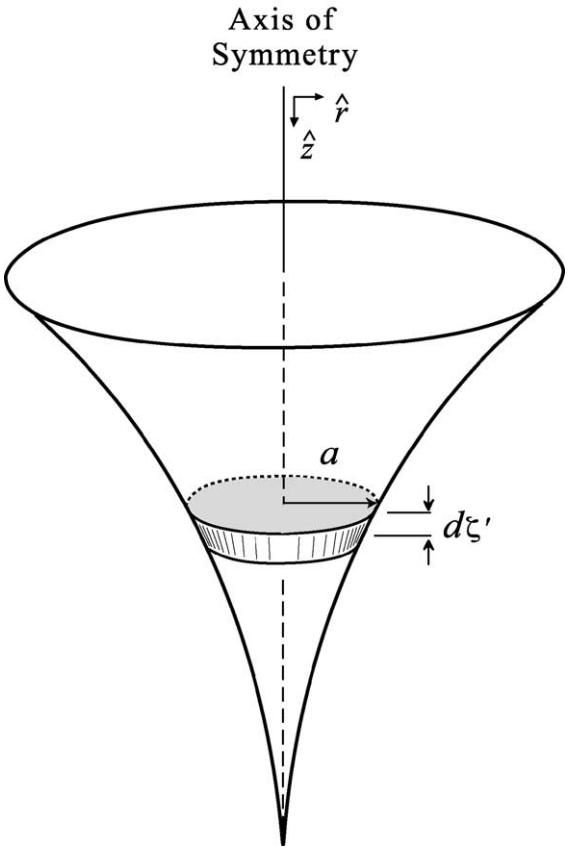

Fig. 4. Schematic diagram illustrating the technique of horizontal circular disks of infinitesimal thickness to approximate the gravitational attraction of a solid of revolution.

where

$$k_2 = \sqrt{\frac{4a[\zeta']r}{(a[\zeta'] + r)^2 + (\zeta' - z)^2}},$$

$a[\zeta']$ is the radius of the outer surface of the solid as a function of vertical length, and other variables as previously defined.

We note that the numerical technique based on cylindrical shells as given by Eq. (3) is easier to implement compared to that based on disks since it requires only the evaluation of a single integral containing an elliptic integral of the first kind. For the case of radial variation of density, the latter technique requires the evaluation of a double integral (i.e., integration of Eq. (45) in Part 1) while for constant density, it involves integrating both an elliptic integral of the first kind and the lambda function (e.g., Eq. (5)).

3. Demonstration of technique based on cylindrical shells

An example involving the gravitational attraction of volcanic islands is presented to demonstrate the technique based on cylindrical shells. Figs. 5 and 6 give Bouguer anomaly values for the islands of Mauke and Mitiaro, respectively, which belong to the Southern Cook Group of islands in the Pacific Ocean (see Robertson, 1967a,b). The values were computed from observed gravity by applying free-air, Bouguer and terrain corrections and subtracting normal gravity as defined by the 1930 International Gravity Formula. Bouguer and terrain corrections were based on densities of 2.67 and 2.30 g/cm^3 for areas of volcanic rock and coral, respectively. Sea water, however, was not replaced by rock and, therefore, the reduced values represent the distribution of mass below sea level.

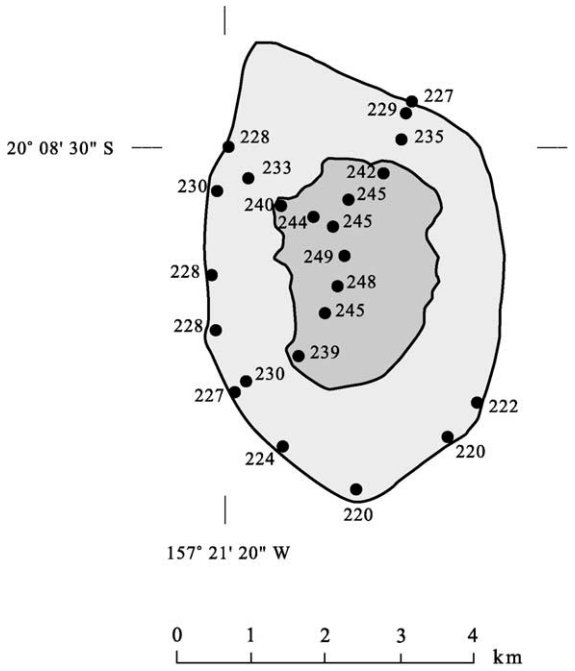

Fig. 5. Bouguer anomaly values (mGal) for the island of Mauke. The central portion of the island (average radius of 1.3 km) consists of weathered basalt (denoted by dark shade) at elevation of about 30 m above sea level and is surrounded by a coral platform (denoted by light shade) at about 20 m. The radius of a circle of an equivalent area that lies inside the outer reef's edge for the entire island is $R = 2.51$ km (modified from Robertson, 1967b).

Fig. 7 depicts an idealized model of an uncompensated island platform consisting of a circular volcanic island (cylindrical core) bounded by an outer platform (exponentially trending surface lying below sea level). The top and bottom surfaces of the model are described by (see Robertson, 1967a, noting change in coordinate origin; Robertson and Kibblewhite, 1966)

$$Z_t[r', z;\ \zeta]_{r' \le R} = 0$$

$$Z_t[r', z;\ \zeta]_{r' \ge R} = H\{1 - \exp[C(R - r')]\}$$

$$Z_b[r', z;\ \zeta] = H$$

where H is the depth to the surrounding ocean floor (=4.6 km), R is the radius of a circle of equivalent area that lies inside of the outer reef's edge for a given island (=2.51 and 2.76 km for Mauke and Mitiaro, respectively), and C is an empirically derived constant that describes the topography of the top surface (=0.10 and 0.11 km^{-1} for Mauke and Mitiaro, respectively).

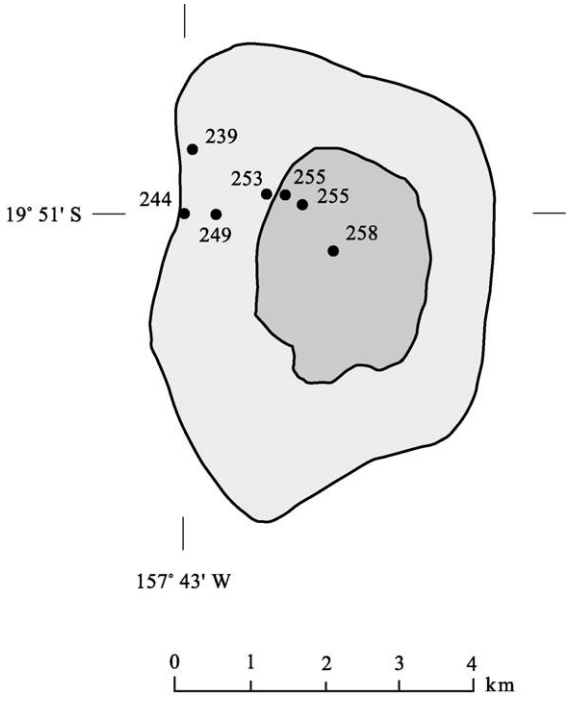

Fig. 6. Bouguer anomaly values (mGal) for the island of Mitiaro. The central portion of the island (average radius of 1.3 km) consists of weathered basalt (denoted by dark shade) at elevation of about 10 m above sea level and is surrounded by a coral platform (denoted by light shade) at about 6 m. The radius of a circle of an equivalent area that lies inside the outer reef's edge for the entire island is R=2.76 km (modified from Robertson, 1967b).

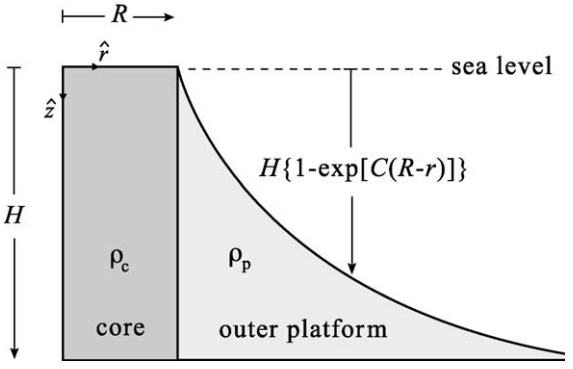

Fig. 7. Idealized representation of an uncompensated island platform. The platform consists of an inner circular volcanic island of radius R and constant density ρ_c (cylindrical core denoted by dark shade) that is surrounded by an outer platform of constant density ρ_p (denoted by light shade). The top surface of the outer platform is described by an exponential function where C is an empirically derived constant and H is the depth to the surrounding ocean floor.

Two general cases have been considered for modelling: (1) the core and outer platform have the same constant density and (2) the core and outer platform have constant but different densities. The solution for the latter case with observations on the island (i.e., $r \le R$) and at sea level (i.e., $\zeta - z = 0$) is the sum of the following two components.

attraction due to cylindrical core:

$$g_z[r, z]_{r \le R} = 4G\Delta\rho_c \int_0^R \left\{ \frac{K[k_t]}{r + r'} - \frac{K[k_b]}{\sqrt{(r + r')^2 + H^2}} \right\} r' dr'$$

$$= 4G\Delta\rho_c \left\{ RE\left[\frac{r}{R}\right] - \int_0^R \frac{K[k_b]}{\sqrt{(r + r')^2 + H^2}} r' dr' \right\}$$

$$k_t = \frac{\sqrt{4rr'}}{r + r'}, \quad k_b = \sqrt{\frac{4rr'}{(r + r')^2 + H^2}} \qquad (6)$$

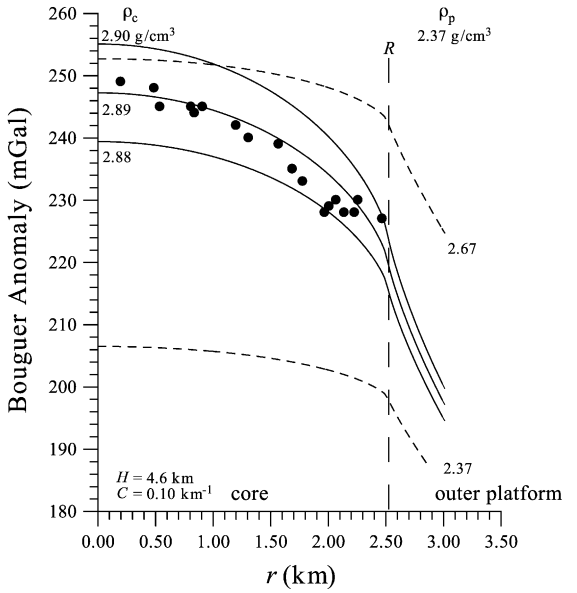

Fig. 8. Modelling results for the island of Mauke. Dashed vertical line denotes island's radius of equivalent area. Solid circles denote Bouguer anomaly values. Solid lines are forward models using the following densities. Upper: $\rho_c = 2.90$ g/cm^3 ($\Delta\rho_c = 1.87$ g/cm^3). Middle: $\rho_c = 2.89$ g/cm^3 ($\Delta\rho_c = 1.86$ g/cm^3). Lower: $\rho_c = 2.88$ g/cm^3 ($\Delta\rho_c = 1.85$ g/cm^3). For all three cases, $\rho_p = 2.37$ g/cm^3 ($\Delta\rho_p = 1.34$ g/cm^3). Upper short-dashed line corresponds to $\rho_c = \rho_p = 2.67$ g/cm^3 ($\Delta\rho_c = \Delta\rho_p = 1.64$ g/cm^3) and lower to $\rho_c = \rho_p = 2.37$ g/cm^3 ($\Delta\rho_c = \Delta\rho_p = 1.34$ g/cm^3).

attraction due to outer platform:

$$g_z[r, z]_{r\le R} = 4G\Delta\rho_p \int_R^{R_{max}} \times \left\{ \frac{K[k_t]}{\sqrt{(r+r')^2 + (H - H\exp[C(R-r')])^2}} - \frac{K[k_b]}{\sqrt{(r+r')^2 + H^2}} \right\} r' dr' \quad (7)$$

$$k_t = \sqrt{\frac{4rr'}{(r+r')^2 + (H - H\exp[C(R-r')])^2}},$$

$$k_b = \sqrt{\frac{4rr'}{(r+r')^2 + H^2}}$$

where $E[r/R]$ is the complete elliptic integral of the second kind (Byrd and Friedman, 1954, Eq. (110.07), p. 10) with modulus r/R, $\Delta\rho_c = \rho_c - \rho_{sw}$ is the contrast in density between the core, ρ_c, and surrounding sea water, ρ_{sw} (= 1.03 g/cm^3), $\Delta\rho_p = \rho_p - \rho_{sw}$ is the contrast in density between the outer platform, ρ_p, and sea water, and R_{max} is the maximum radial distance of the platform. This distance was set to the extrapolated distance to where the platform lies approximately 100 m above the surrounding ocean floor (= 34 and 38 km, for Mauke and Mitiaro, respectively; see Robertson and Kibblewhite, 1966).

An adaptive Simpson's rule (Shampine and Allen, 1973) was used to provide a more efficient numerical integration (as compared to a conventional Simpson's rule) given that the integrands, in general, decrease rapidly with increasing r'. Note that the first term in Eq. (6) is the closed-form solution for the gravitational

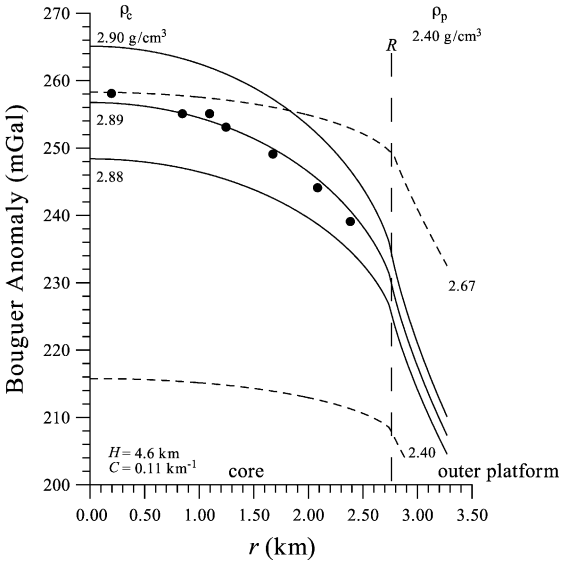

Fig. 9. Modelling results for the island of Mitiaro. Dashed vertical line denotes island's radius of equivalent area. Solid circles denote Bouguer anomaly values. Solid lines are forward models using the following densities. Upper: $\rho_c = 2.90$ g/cm^3 ($\Delta\rho_c = 1.87$ g/cm^3). Middle: $\rho_c = 2.89$ g/cm^3 ($\Delta\rho_c = 1.86$ g/cm^3). Lower: $\rho_c = 2.88$ g/cm^3 ($\Delta\rho_c = 1.85$ g/cm^3). For all three cases, $\rho_p = 2.40$ g/cm^3 ($\Delta\rho_p = 1.37$ g/cm^3). Upper short-dashed line corresponds to $\rho_c = \rho_p = 2.67$ g/cm^3 ($\Delta\rho_c = \Delta\rho_p = 1.64$ g/cm^3) and lower to $\rho_c = \rho_p = 2.40$ g/cm^3 ($\Delta\rho_c = \Delta\rho_p = 1.34$ g/cm^3).

attraction along the surface of a semi-infinite cylinder (see Eq. (A5) in Appendix A).

Figs. 8 and 9 display the results of modelling for Mauke and Mitiaro, respectively. The best-fit models assume a high-density core of 2.89 g/cm^3 ($\Delta\rho_c = 1.86$ g/cm^3) surrounded by a less-dense outer platform of 2.37 and 2.40 g/cm^3, respectively ($\Delta\rho_p = 1.34$ and 1.37 g/cm^3). The modelled density of the core falls within the range of wet density determined for six samples of massive olivine basalt (2.86–3.04 g/cm^3, Robertson, 1967a). The modelled densities for the outer platform are consistent with vesicular and clastic basalts.

The modelling is intended to demonstrate the technique only and the results do not necessarily represent the best fit of the data. More complicated geologic models that include, for example, flexure of an elastic (Brotchie, 1971; McNutt and Menard, 1978) or a viscoelastic (Beaumont, 1978) lithosphere in response to surface loading caused by islands themselves can also be easily accommodated by the proposed technique. Solutions to surface-loading problems are usually given in terms of vertical deflection as a function of radial distance (and time for the viscoelastic case). Using the disk technique to calculate the corresponding gravitational effect would require a recasting of parameters combined with time consuming root-finding in order to perform the necessary integration in the vertical direction. Similarly, the solutions to a variety of other physical problems that are cast in a like manner are also better suited using the procedure based on cylindrical shells (e.g., the gravity response associated with drawdown in an aquifer where the drawdown solution is given as a function of radial distance).

4. Generalization to arbitrary orientation

In the following, a general procedure is outlined to calculate the gravitational attraction of an arbitrarily oriented solid of revolution with constant density. This procedure is based on vector analysis of the vertical and radial components of attraction combined with coordinate transformation. The vertical component is given by Eq. (3) and the radial component (assuming constant density) is derived in Appendix B.

An integral expression for the radial component of gravitational attraction due to a solid of revolution has the form

$$g_r[r, z] = -\frac{2G\rho}{r}\int_{z_t}^{z_b}\left\{\sqrt{(a[\zeta'] + r)^2 + (\zeta' - z)^2} \times \left[\left(1 - \frac{k_2^2}{2}\right)K[k_2] - E[k_2]\right]\right\}d\zeta' \quad (8)$$

where the variables are as previously defined. This solution, based on the disk technique, contains only complete elliptic integrals of the first and second kinds and thus is easier to numerically implement as compared to an equivalent expression based on cylindrical shells which requires integrating the lambda function (see Eqs. (B6a–6c) in Appendix B). Taken together, Eqs. (3) and (8) provide the requisite vector components needed to calculate the attraction of an arbitrarily oriented solid using the following scheme.

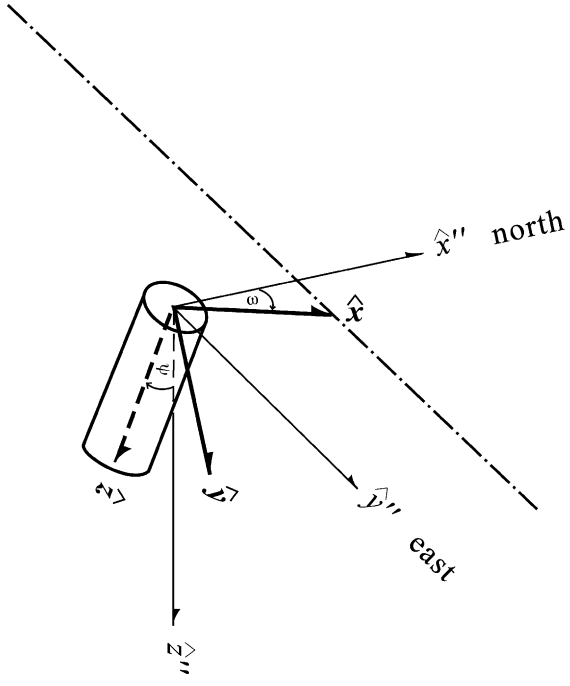

Fig. 10. Body (unprimed) and survey (double primed) coordinate systems adopted for an inclined solid of revolution. The azimuth, ω, is the angle between north and the $\hat{x}$ axis. The deviation, ψ, is the angle between vertical and the $\hat{z}$ axis as measured in the xz plane.

Initially, define two right-handed coordinate systems (termed body and survey) that have a common origin located at the top and center of the solid (i.e., $\zeta = \zeta'' = 0$) as depicted in Fig. 10. For convenience, unprimed notation is adopted for the body system and double-primed notation for the survey system. The $\hat{z}$ axis is defined to coincide with the rotational axis of the body while for the survey system, the $\hat{x}''$, $\hat{y}''$ and $\hat{z}''$ axes correspond to north, east and vertically downwards, respectively. Further, define an azimuth, ω, as the angle between north and the $\hat{x}$ axis, and a *deviation*, ψ, as the angle between vertical and the $\hat{z}$ axis as measured in the xz plane. The positive sense of both ω and ψ is *counterclockwise* as viewed toward the origin along the negative direction of $\hat{z}$ and $\hat{x}$, respectively.

The coordinates of an observation point in the survey system (x'', y'', z'') are translated to the body system (r, z) according to

$$\begin{bmatrix} x \\ y \\ z \end{bmatrix} = \begin{bmatrix} \cos\omega & \sin\omega & 0 \\ -\sin\omega\cos\psi & \cos\omega\cos\psi & \sin\psi \\ \sin\omega\sin\psi & -\cos\omega\sin\psi & \cos\psi \end{bmatrix} \begin{bmatrix} x'' \\ y'' \\ z'' \end{bmatrix} \tag{9}$$

where $r = \sqrt{x^2 + y^2}$. Eqs. (3) and (8) are now used to calculate the vertical and radial components of gravitational attraction in the body system, noting that $g_x[x, y, z] = g_r[r, \theta]\cos\theta$ and $g_y[x, y, z] = g_r[r, \theta]\sin\theta$, where $\theta = \tan^{-1}[y/x]$. The gravitational attraction in the survey system is determined by using the inverse of the 3×3 matrix in Eq. (9) such that

$$\begin{bmatrix} g_{x''} \\ g_{y''} \\ g_{z''} \end{bmatrix} = \begin{bmatrix} \cos\omega & -\sin\omega\cos\psi & \sin\omega\sin\psi \\ \sin\omega & \cos\omega\cos\psi & -\cos\omega\sin\psi \\ 0 & \sin\psi & \cos\psi \end{bmatrix} \begin{bmatrix} g_x \\ g_y \\ g_z \end{bmatrix} \tag{10}$$

from which

$$g_{x''} = g_x\cos\omega - g_y\sin\omega\cos\psi + g_z\sin\omega\sin\psi, \tag{11}$$

$$g_{y''} = g_x\sin\omega + g_y\cos\omega\cos\psi - g_z\cos\omega\sin\psi, \tag{12}$$

and

$$g_{z''} = g_y\sin\psi + g_z\cos\psi. \tag{13}$$

For brevity, the notation for the functional arguments has been omitted in the above expressions and will be excluded hereafter.

As an example, Fig. 11 shows the results of modelling an inclined finite-length cylinder with $\omega = 0$ and ψ ranging between 0 (i.e., rotational axis oriented vertically) and 90° (i.e., rotational axis lying horizontally in the yz plane). For convenience, we have defined the deviation to be relative to the rotational axis of a vertically oriented cylinder and not according to the general geologic definition of dip which is the angle with respect to the horizontal plane. For the latter definition to apply, one needs to replace ψ in Eqs. (3.9) and (3.10) with $-(\psi - 90°)$.

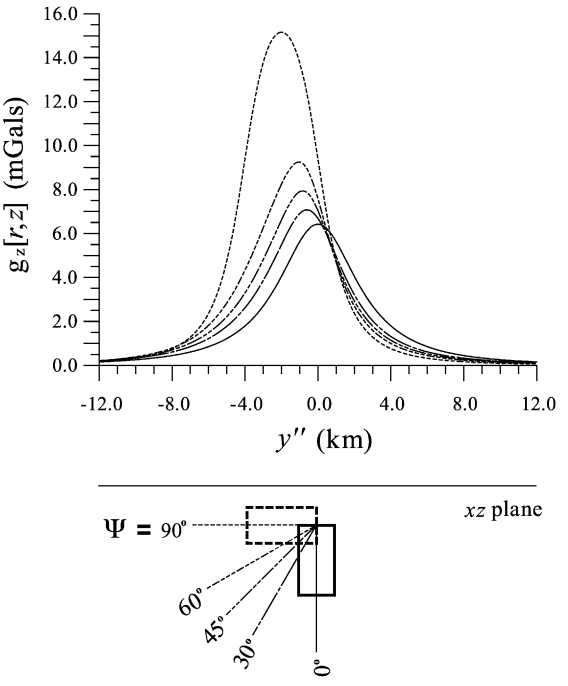

Fig. 11. Vertical gravitational attraction of an inclined finite-length cylinder for various values of deviation, ψ, and with the following parameters: density contrast, $\Delta\rho = 1$ g/cm^3; depth to center of top of cylinder, $|z''| = 2$ km; radius, $a = 1$ km; length, $l = 4a = 4$ km; and azimuth, $\omega = 0°$.

The present scheme is particularly convenient for modelling the vertical gravitational attraction of a finite-length horizontal cylinder. This attraction (Eq. (13) with $\psi = 90°$) is given as

$$\begin{aligned} g_{z''} &= g_y \\ &= g_r \sin\theta \\ &= -\frac{2G\rho\sin\theta}{r}\int_0^l \left\{\sqrt{(a+r)^2+(\zeta-z)^2}\right. \\ &\quad \left.\times\left[\left(1-\frac{k_1^2}{2}\right)K[k_1]-E[k_1]\right]\right\}\mathrm{d}\zeta \end{aligned} \tag{14}$$

where l is the length of the cylinder. This solution is easy to numerically implement. Alternatively, a closed-form solution can be derived using Eq. (B3c) (see Appendix B) and superposition to yield

$$\begin{aligned} g_{z''} = \frac{G\rho\sin\theta}{r}&\left\{\frac{\pi}{2}(r^2-a^2)(\Lambda_0[\phi,\,k_\mathrm{b}]-\Lambda_0[\phi,\,k_\mathrm{t}])\right. \\ &+(z_\mathrm{b}-z)\sqrt{(a+r)^2+(z_\mathrm{b}-z)^2} \\ &\times\left(E[k_\mathrm{b}]-\frac{2a^2+2r^2+(z_\mathrm{b}-z)^2}{(a+r)^2+(z_\mathrm{b}-z)^2}K[k_\mathrm{b}]\right) \\ &-(z_\mathrm{t}-z)\sqrt{(a+r)^2+(z_\mathrm{t}-z)^2} \\ &\left.\times\left(E[k_\mathrm{t}]-\frac{2a^2+2r^2+(z_\mathrm{t}-z)^2}{(a+r)^2+(z_\mathrm{t}-z)^2}K[k_\mathrm{t}]\right)\right\} \end{aligned} \tag{15}$$

where

$$k_\mathrm{b} = \sqrt{\frac{4ar}{(a+r)^2+(z_\mathrm{b}-z)^2}} \text{ and}$$

$$k_\mathrm{t} = \sqrt{\frac{4ar}{(a+r)^2+(z_\mathrm{t}-z)^2}}.$$

Fig. 12 gives percent differences between solutions for finite-length and infinite-length horizontal cylinders. The latter is commonly used in modelling to approximate a variety of features such as anticlines and tunnels. The comparison indicates that significant errors may result when using the infinite-length solution to model finite-length features.

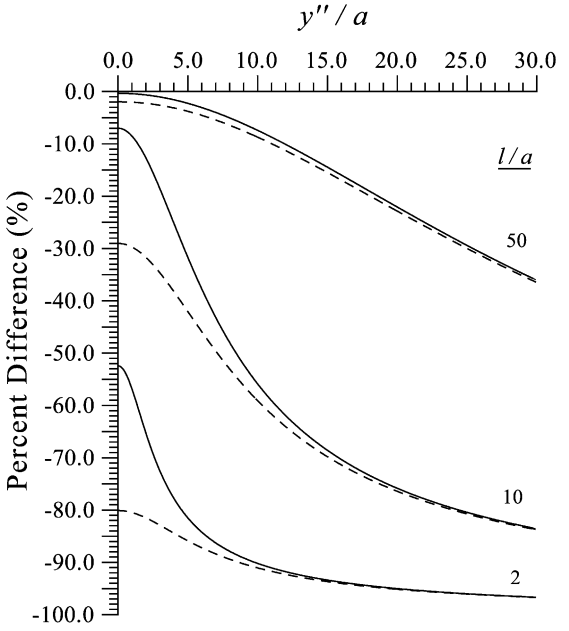

Fig. 12. Percent difference in vertical gravitational attraction versus normalized perpendicular distance (i.e., along $\hat{y}''$ axis) between finite- and infinite-length horizontal cylinders. Each pair of solid and dashed curves corresponds to a specific normalized length, l/a, of cylinder. Also, solid curves correspond to a normalized depth-to-center of cylinder, $|z''|/a = 2$, while the dashed curves $= 5$. Calculations were made along profiles that were oriented perpendicular to the midpoint for each finite-length cylinder (e.g., for the upper pair of curves with $l/a = 50$, calculations were made for a profile crossing the midpoint at 25).

5. Extension to magnetic case

The static magnetic field due to a magnetized solid of revolution can be derived from its gravitational field through Poisson's relation which can be written as (Garland, 1951; Grant and West, 1965, Eq. (8-4), p. 213)

$$\mathbf{F}_t = \frac{M_t}{G\rho}\frac{\partial}{\partial\alpha_t}\mathbf{g} \tag{16}$$

where $\mathbf{F}_t$ is the anomalous magnetic field intensity, either remanent (t = "p") or induced (t = "i"), M_t is magnetization and α_t is in the direction of magnetization. The above relation assumes a homogenous

mass distribution in which both M_t and ρ are constant throughout the body. Note that for the magnetic case, it is convenient to define a right-handed coordinate system such that $\hat{x}''$ is directed towards magnetic north (and not geographic north as was adopted for the case of gravity) and $\hat{z}''$ is positive downward. We have retained the double-primed notation for the survey coordinate system to avoid confusion with the systems that have been previously defined for the case of gravity.

For the moment, consider induced magnetization only. The direction cosines are

$$\frac{\partial}{\partial \alpha_i} = \mathsf{l}\frac{\partial}{\partial x''} + \mathsf{m}\frac{\partial}{\partial y''} + \mathsf{n}\frac{\partial}{\partial z''} \tag{17}$$

where $\mathsf{l} = \cos I_0 \cos D_0$, $\mathsf{m} = \cos I_0 \sin D_0$, $\mathsf{n} = \sin I_0$ and (D_0, I_0) are the magnetic declination and inclination of the Earth's field, respectively. Substitution of Eq. (17) into Eq. (16) yields the following expressions for the components of the anomalous magnetic field intensity

$$\Delta X_i'' = \frac{M_i}{G\rho}\left\{\mathsf{l}\frac{\partial}{\partial x''} + \mathsf{m}\frac{\partial}{\partial y''} + \mathsf{n}\frac{\partial}{\partial z''}\right\} g_{x''} \tag{18}$$

$$\Delta Y_i'' = \frac{M_i}{G\rho}\left\{\mathsf{l}\frac{\partial}{\partial x''} + \mathsf{m}\frac{\partial}{\partial y''} + \mathsf{n}\frac{\partial}{\partial z''}\right\} g_{y''} \tag{19}$$

and

$$\Delta Z_i'' = \frac{M_i}{G\rho}\left\{\mathsf{l}\frac{\partial}{\partial x''} + \mathsf{m}\frac{\partial}{\partial y''} + \mathsf{n}\frac{\partial}{\partial z''}\right\} g_{z''}. \tag{20}$$

The total anomalous magnetic field intensity due to induced magnetization is given as

$$\Delta T_i'' = \sqrt{\Delta X_i''^2 + \Delta Y_i''^2 + \Delta Z_i''^2}. \tag{21}$$

For a body with vertical magnetization ($I_0 = 90°$, $\mathsf{l} = \mathsf{m} = 0$, $\mathsf{n} = 1$), Eq. (21) reduces to

$$\Delta T_i'' = \frac{M_i}{G\rho}\left\{\sqrt{\left(\frac{\partial g_{x''}}{\partial z''}\right)^2 + \left(\frac{\partial g_{y''}}{\partial z''}\right)^2 + \left(\frac{\partial g_{z''}}{\partial z''}\right)^2}\right\}. \tag{22}$$

A similar set of expressions can be written for remanent magnetization. The direction cosines are

$$\frac{\partial}{\partial \alpha_p} = \mathsf{L}\frac{\partial}{\partial x''} + \mathsf{M}\frac{\partial}{\partial y''} + \mathsf{N}\frac{\partial}{\partial z''} \tag{23}$$

where $\mathsf{L} = \cos I \cos D$, $\mathsf{M} = \cos I \sin D$, $\mathsf{N} = \sin I$ and (D, I) are the magnetic declination and inclination of the remanent magnetization, respectively. The total anomalous magnetic field intensity can be obtained from the vector sum of the induced and remanent components.

The magnetic effects due to solids of revolution can be numerically calculated in a straightforward manner by incorporating the expressions for gravity that were derived in the previous section. Solutions for a vertical cylinder and horizontal circular lamina have been given by Singh and Sabina (1978) and Singh et al. (1979), respectively.

6. Concluding remarks

Simple integral expressions have been formulated and a numerical technique presented to describe the gravitational attraction due to any solid of revolution. The technique is easy to implement and only requires algorithms that are readily available. The main advantage of the technique is that numerical integration is performed with respect to the radial direction as opposed to the vertical. As a result, axisymmetric solutions that describe various physical problems (e.g., gravitational effect due to lithospheric deflection near seamounts, gravitational response associated with hydraulic testing of groundwater aquifers, etc.) are easily handled that otherwise would require time consuming root finding using existing techniques that are based on disk-type solutions. Solids with complicated geometry or consisting of composite shapes—such as the modelling of volcanic islands—are easily accommodated through superposition. In addition, the technique can be used to determine the attraction of solids with constant density and arbitrary orientation through coordinate transformation that considers both vertical and radial components of attraction. An example of this case is an inclined finite-length cylinder which can be used to model the effects of tunnels.

Acknowledgements

The authors wish to thank Dr. Stephen Park for discussions on the topic, and Drs. Peter Furness and

Niels Christensen for their constructive comments on the manuscript.

Appendix A. Gravitational attraction of solids of revolution: parameters and special cases

The use of solids of revolution, although in some instances a gross simplification, is instructive in forward gravity modelling various geological features. Examples include mountains and volcanoes (cone), atolls and guyots (frustum), salt domes, batholiths and solution cavities (cylinder), circular depressions such as impact craters and lakes (inverted cap) and volcanic roots (inverted cone).

Table A1 lists the defining parameters needed to numerically evaluate the vertical component of gravitational attraction for various solids of revolution using Eq. (3). Table A2 lists the parameters to calculate the radial component using Eq. (8). Figs. A1–9 provide schematic diagrams with appropriate notation for these solids. Finally, Eqs. (A1–37) are special solutions that are given without derivation. Some of these are cross-referenced with equivalent solutions available in the literature. Note that P denotes the point of observation.

A.1. Vertical semi-infinite circular cylinder

P along vertical axis ($r=0,\ \rho'[r']=\rho_0(A+Br'+Cr'^2)$).

$$g_z[0,z;\ \zeta] = 2\pi G\rho_0\left\{\left(A+\frac{Ba}{2}-C(\zeta-z)^2\right)\times\sqrt{a^2+(\zeta-z)^2}-A(\zeta-z)+\frac{B(\zeta-z)^2}{2}\ln\left[\frac{\zeta-z}{a+\sqrt{a^2+(\zeta-z)^2}}\right]+\frac{2C}{3}(\zeta-z)^3+\frac{C}{3}\left[a^2+(\zeta-z)^2\right]^{3/2}\right\} \tag{A1}$$

where ρ_0 is density at the center and the units of A, B and C are dimensionless, L^{-1}, and L^{-2}, respectively.

Table A1
Parameters for calculating the vertical component of gravitational attraction for various solids of revolution

Solid of revolution	Figure	Limits of integral	$Z_t[r']$	$Z_b[r']$
Right circular cylinder	Fig. 1 (Part 1)	$0\rightarrow a$	b	$b+l$
Right circular cone	Fig. A1	$0\rightarrow a_b$	$b+r'\dfrac{l}{a_b}$	$b+l$
Frustum[a]	Fig. A2	$0\rightarrow a_t$	$b+c$	$b+c+l$
		$a_t\rightarrow a_b$	$b+r'\dfrac{c}{a_t}$	$b+c+l$
Inverted right circular cone	Fig. A3	$0\rightarrow a_t$	b	$b+l-r'\dfrac{l}{a_t}$
Inverted frustum[b]	Fig. A4	$0\rightarrow a_b$	b	$b+l$
		$a_b\rightarrow a_t$	b	$b+l+c-r'\dfrac{c}{a_b}$
Spherical cap	Fig. A5	$0\rightarrow\sqrt{2a_sl-l^2}$	$b-\sqrt{a_s^2-r'^2}$	$b-a_s+l$
Inverted spherical cap	Fig. A5	$0\rightarrow\sqrt{2a_sl-l^2}$	$b+a_s-l$	$b+\sqrt{a_s^2-r'^2}$
Oblate or prolate spheroid	Fig. A6 and Fig. A8	$0\rightarrow h$	$b-\dfrac{v}{h}\sqrt{h^2-r'^2}$	$b+\dfrac{v}{h}\sqrt{h^2-r'^2}$
Oblate or prolate spheroidal cap	Fig. A7 and Fig. A9	$0\rightarrow\dfrac{h}{v}\sqrt{2vl-l^2}$	$b-\dfrac{v}{h}\sqrt{h^2-r'^2}$	$b-v+l$
Inverted oblate or prolate spheroidal cap	Fig. A7 and Fig. A9	$0\rightarrow\dfrac{h}{v}\sqrt{2vl-l^2}$	$b+v-l$	$b+\dfrac{v}{h}\sqrt{h^2-r'^2}$

[a] Two integrals are required to define the top surface.
[b] Two integrals are required to define the bottom surface.

Table A2
Parameters for calculating the radial component of gravitational attraction for various solids of revolution

Solid of revolution	Figure	Limits of integral	$a[\zeta']$
Right circular cylinder	Fig. 1 (Part 1)	$b \rightarrow b+l$	a
Right circular cone	Fig. A1	$b \rightarrow b+l$	$(\zeta'-b)\frac{a_b}{l}$
Frustum	Fig. A2	$b+c \rightarrow b+c+l$	$(\zeta'-b)\frac{a_t}{c}$
Inverted right circular cone	Fig. A3	$b \rightarrow b+l$	$(b+l-\zeta')\frac{a_t}{l}$
Inverted frustum	Fig. A4	$b \rightarrow b+l$	$(b+l+c-\zeta')\frac{a_b}{c}$
Spherical cap	Fig. A5	$b-a_s \rightarrow b-a_s+l$	$\sqrt{a_s^2-(b-\zeta')^2}$
Inverted spherical cap	Fig. A5	$b+a_s-l \rightarrow b+a_s$	$\sqrt{a_s^2-(\zeta'-b)^2}$
Oblate or prolate spheroid[a]	Fig. A6 and Fig. A8	$b-v \rightarrow b$	$\frac{h}{v}\sqrt{v^2-(b-\zeta')^2}$
		$b \rightarrow b+v$	$\frac{h}{v}\sqrt{v^2-(\zeta'-b)^2}$
Oblate or prolate spheroidal cap	Fig. A7 and Fig. A9	$b-v \rightarrow b-v+l$	$\frac{h}{v}\sqrt{v^2-(b-\zeta')^2}$
Inverted oblate or prolate spheroidal cap	Fig. A7 and Fig. A9	$b+v-l \rightarrow b+v$	$\frac{h}{v}\sqrt{v^2-(\zeta'-b)^2}$

[a] Two integrals are required to define radial variation.

P at center of top surface ($r=0,\ z=\zeta,\ \rho'[r']=\rho_0(A+Br'+Cr'^2)$).

$$g_z[0,\ \zeta;\ \zeta] = 2\pi G\rho_0\left\{Aa+\frac{Ba^2}{2}+\frac{Ca^3}{3}\right\} \tag{A2}$$

P at edge of top surface ($r=a,\ z=\zeta,\ \rho'[r']=\rho_0(A+Br'+Cr'^2)$).

$$g_z[a,\ \zeta;\ \zeta] = 4G\rho_0 a\left\{A+\frac{Ba}{2}\left(\frac{1}{2}+\overline{\bar{G}}\right)+\frac{5Ca^2}{9}\right\} \tag{A3}$$

where $\overline{G}$ is Catalan's constant (≈ 0.91596559).

P along top surface ($\rho'[r']=\rho=$ constant).

$$g_z[r,\ \zeta;\ \zeta] = 2G\rho\left\{(a-r)K\left[\frac{\sqrt{4ar}}{a+r}\right]+(a+r)E\left[\frac{\sqrt{4ar}}{a+r}\right]\right\} \tag{A4}$$

(Nabighian, 1962, Eq. (9))

$$g_z[r,\ \zeta;\ \zeta]_{r\le a} = 4G\rho aE\left[\frac{r}{a}\right] \tag{A5}$$

(Talwani, 1973, Eq. (39))

$$g_z[r,\ \zeta;\ \zeta]_{r\ge a} = 4G\rho\left\{(a+r)E\left[\frac{\sqrt{4ar}}{a+r}\right]-rE\left[\frac{a}{r}\right]\right\} \tag{A6}$$

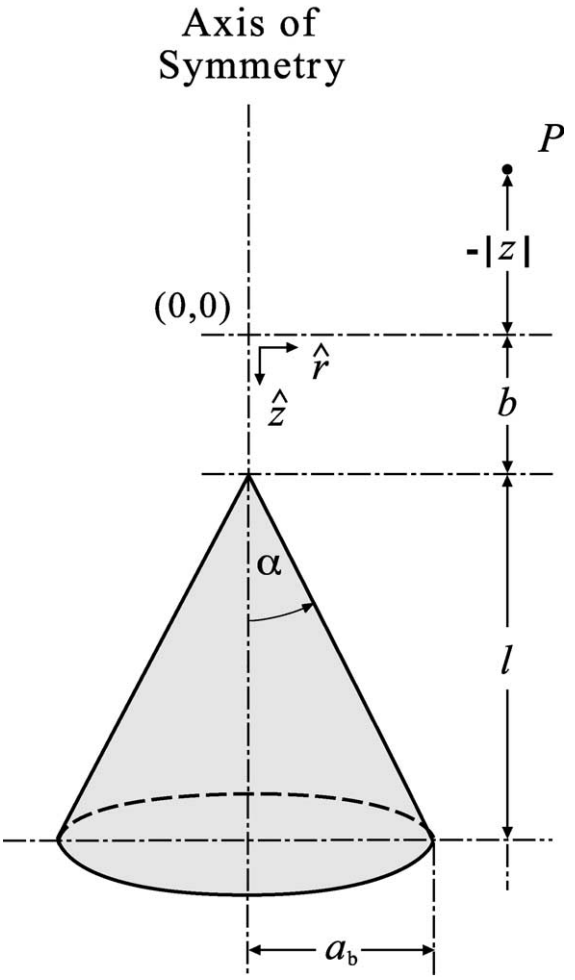

Fig. A1. Schematic diagram for right circular cone.

$$g_z[r,\ \zeta;\ \zeta]_{r\geq a} = 4G\rho r\left\{E\left[\frac{a}{r}\right] - \left(1-\frac{a^2}{r^2}\right)K\left[\frac{a}{r}\right]\right\} \tag{A7}$$

(Singh, 1977, Eq. (8))

P at edge of top surface ($r=a$, $\zeta - z = 0$, $\rho'[r'] = \rho =$ constant).

$$g_a[z,\ \zeta;\ \zeta] = 4G\rho a \tag{A8}$$

P along vertical edge ($r=a$, $\rho'[r'] = \rho =$ constant).

$$g_z[a,\ z;\ \zeta] = 2G\rho\left\{\sqrt{4a^2+(\zeta-z)^2}E[k_1] - \frac{\pi}{2}(\zeta - z)\right\} \tag{A9}$$

(Talwani, 1973, Eq. (35))

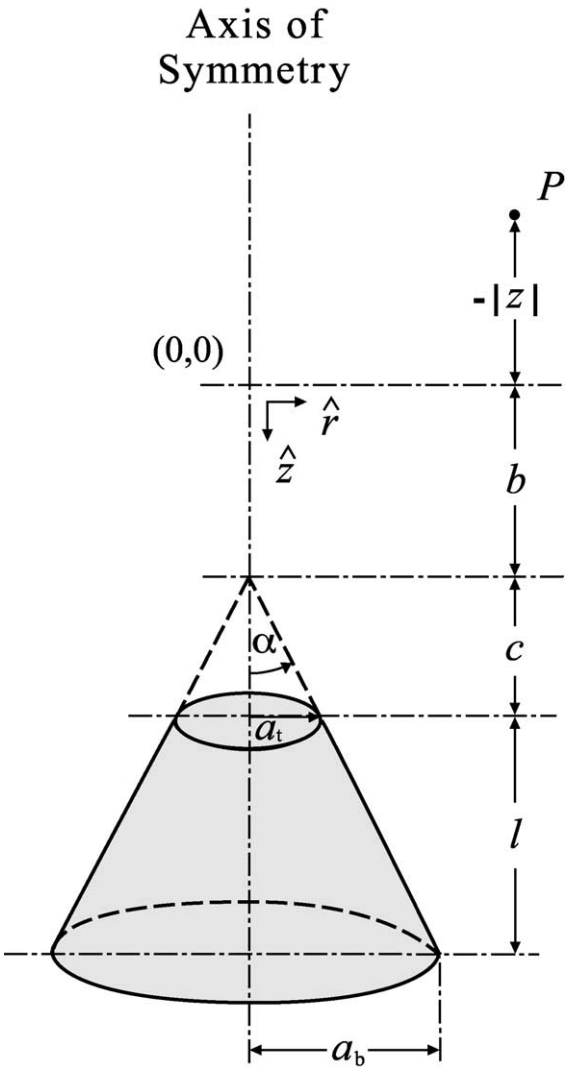

Fig. A2. Schematic diagram for frustum.

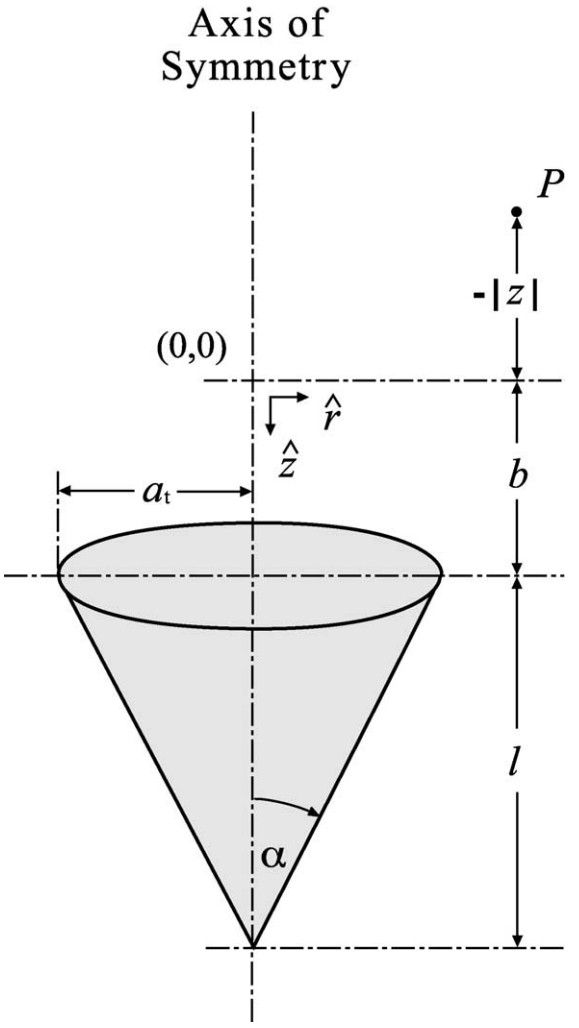

Fig. A3. Schematic diagram for inverted right circular cone.

A.2. Right circular cone

P along vertical axis ($r=0$, $\rho'[r']=\rho=$constant).

$$g_z[0,z]=2\pi G\rho\left\{l-[\overline{A}-(b-z)]\times\cos^2\alpha\pm(b-z)\sin^2\alpha\cos\alpha\times\ln\left[\frac{(b-z)(1\pm\cos\alpha)}{\overline{A}\pm\sqrt{a_b^2+l^2}\pm(b-z)\cos\alpha}\right]\right\} \tag{A10}$$

$$g_z[0,z]=2\pi G\rho\left\{l-[\overline{A}-(b-z)]\times\cos^2\alpha\pm(b-z)\sin^2\alpha\cos\alpha\times\ln\left[\frac{\overline{A}\mp\sqrt{a_b^2+l^2}\mp(b-z)\cos\alpha}{(b-z)(1\mp\cos\alpha)}\right]\right\} \tag{A11}$$

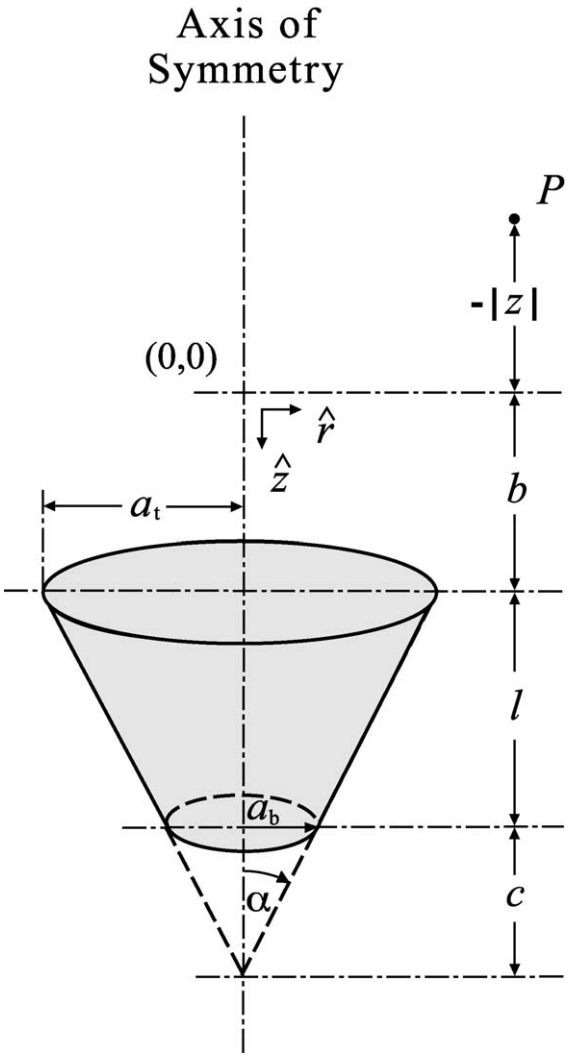

Fig. A4. Schematic diagram for inverted frustum.

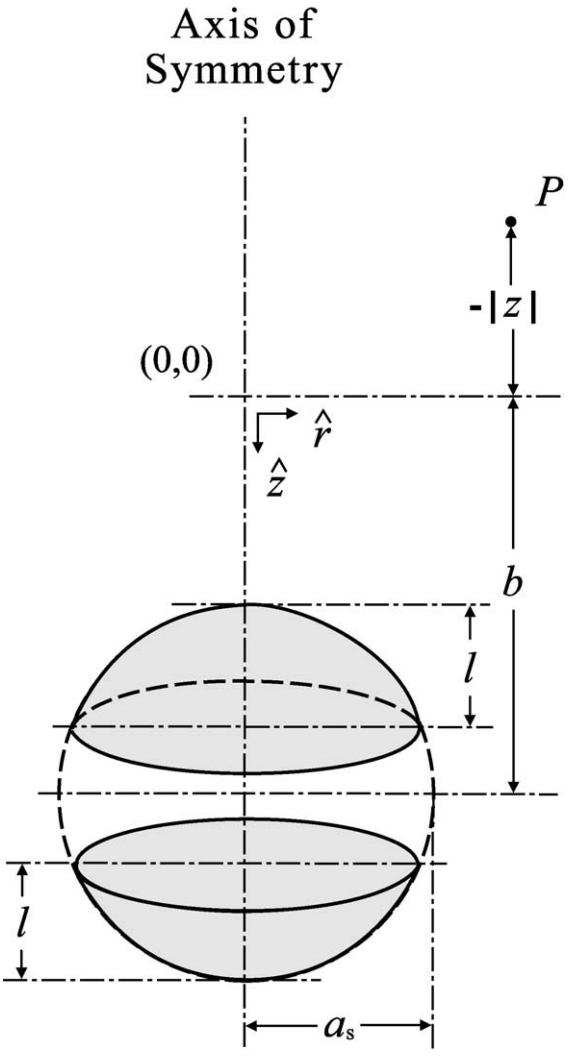

Fig. A5. Schematic diagram for spherical and inverted spherical caps.

where $\overline{A} = \sqrt{a_b^2 + (b - z + l)^2}$. Duska (1958, Eq. (5)) gives one form of this solution with $\rho = a_b$, $d = b - z$, $H = \sqrt{a_b^2 + l^2}$ and $r_1 = \sqrt{a_b^2 + (b - z + l)^2}$.

P at vertex ($r = 0$, $b - z = 0$, $\rho'[r'] = \rho = \text{constant}$).

$$g_z[0, z] = 2\pi G\rho l(1 - \cos\alpha) = 2\pi G\rho\left\{1 - \frac{l}{\sqrt{a_b^2 + l^2}}\right\} \quad \text{(A12)}$$

A.3. Frustum

P along vertical axis ($r = 0$, $\rho'[r'] = \rho = \text{constant}$).

$$g_z[0, z] = 2\pi G\rho\left\{l - (\overline{A} - \overline{B})\cos\alpha \pm (b - z)\cos\alpha\sin^2\alpha \times \ln\left[\frac{\overline{B} \pm \sqrt{a_t^2 + c^2} \pm (b - z)\cos\alpha}{\overline{A} \pm \sqrt{a_b^2 + (c + l)^2} \pm (b - z)\cos\alpha}\right]\right\} \quad \text{(A13)}$$

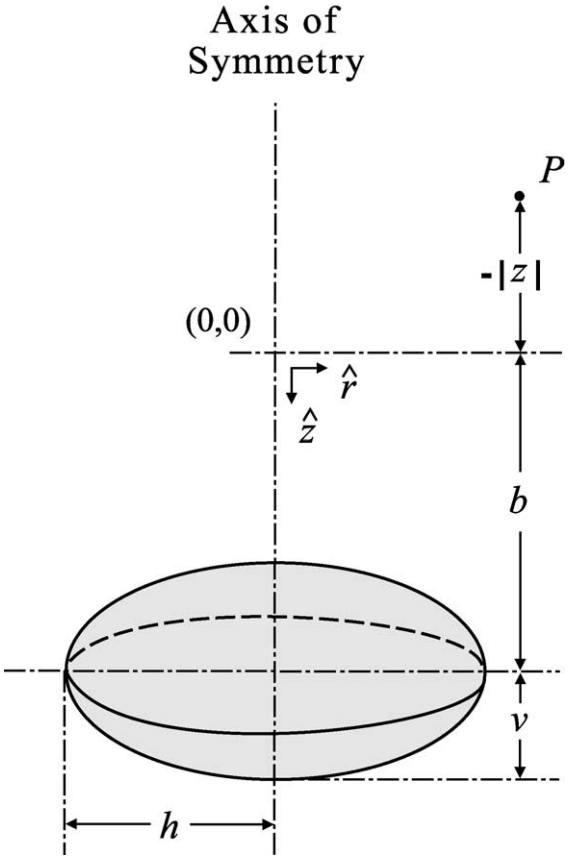

Fig. A6. Schematic diagram for oblate spheroid.

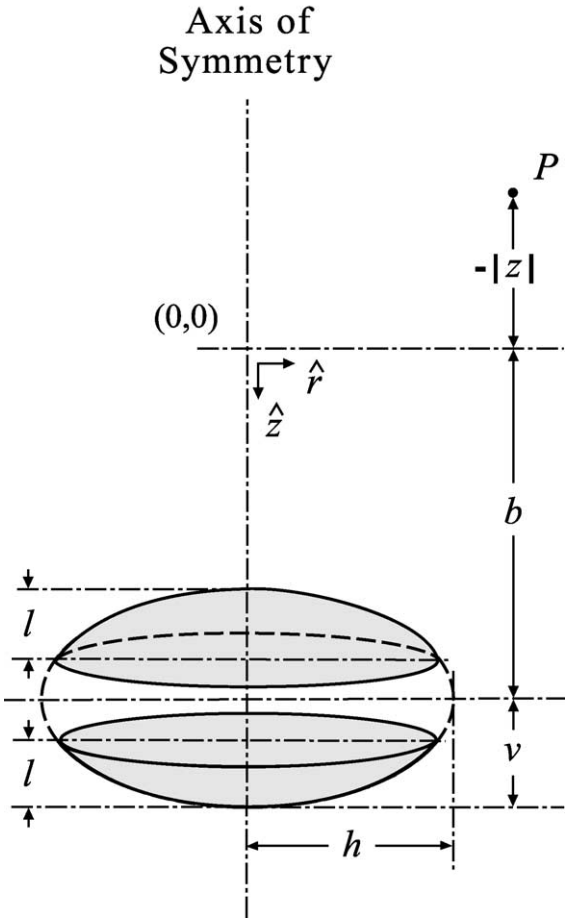

Fig. A7. Schematic diagram oblate and inverted oblate spheroidal caps.

$$g_z[0,\,z] = 2\pi G\rho\left\{ l - (\overline{A} - \overline{B})\cos\alpha \pm (b-z)\cos\alpha \right.$$
$$\left. \times \sin^2\alpha \ln\left[\frac{\overline{A} \mp \sqrt{a_b^2 + (c+l)^2} \mp (b-z)\cos\alpha}{\overline{B} \mp \sqrt{a_t^2 + c^2} \mp (b-z)\cos\alpha} \right] \right\} \quad \text{(A14)}$$

where $\overline{A} = \sqrt{a_b^2 + (b-z+c+l)^2}$ and $\overline{B} = \sqrt{a_t^2 + (b-z+c)^2}$. Duska (1958, Eq. (7)) gives one form of this solution with $\beta = \alpha$, $\rho_u = a_t$, $\rho_l = a_b$, $a = l$, $c = b - z + c$, $d = b - z$, $r_l = \overline{A}$ and $r_u = \overline{B}$.

P at centerpoint of top surface ($r = 0$, $b + c - z = 0$, $\rho'[r'] = \rho = \text{constant}$).

$$g_z[0,\,z] = 2\pi G\rho\left\{ l - \left[\sqrt{a_b^2 + l^2} - a_t\right]\cos\alpha + c\sin^2\alpha \right.$$
$$\left. \times \cos\alpha \ln\left[\frac{\sqrt{a_b^2 + l^2}\cos\alpha + c\sin^2\alpha + l}{a_t\cos\alpha + c\sin^2\alpha} \right] \right\} \quad \text{(A15)}$$

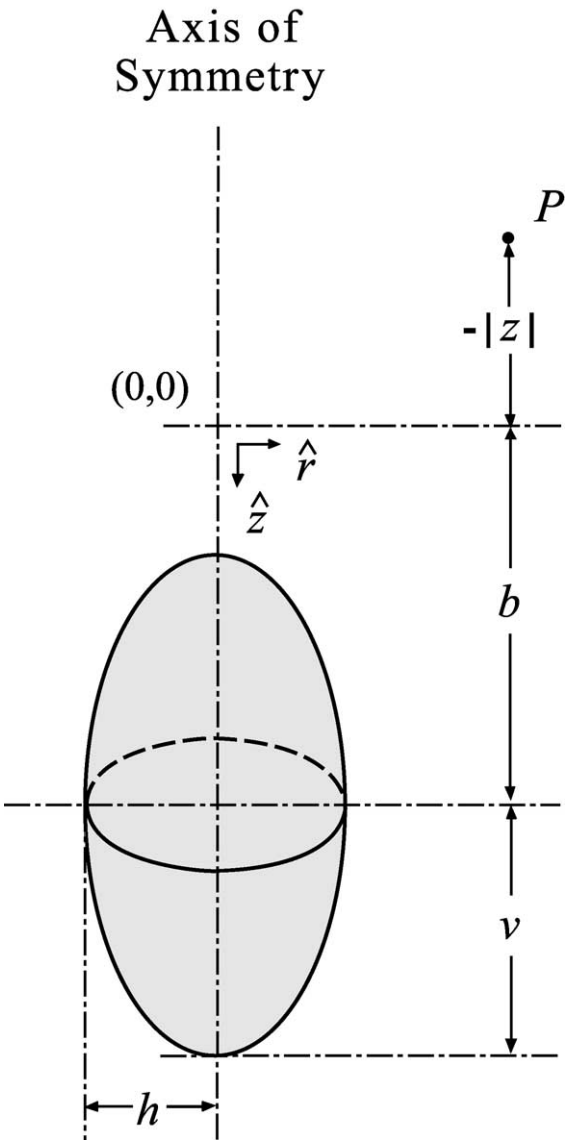

Fig. A8. Schematic diagram for prolate spheroid.

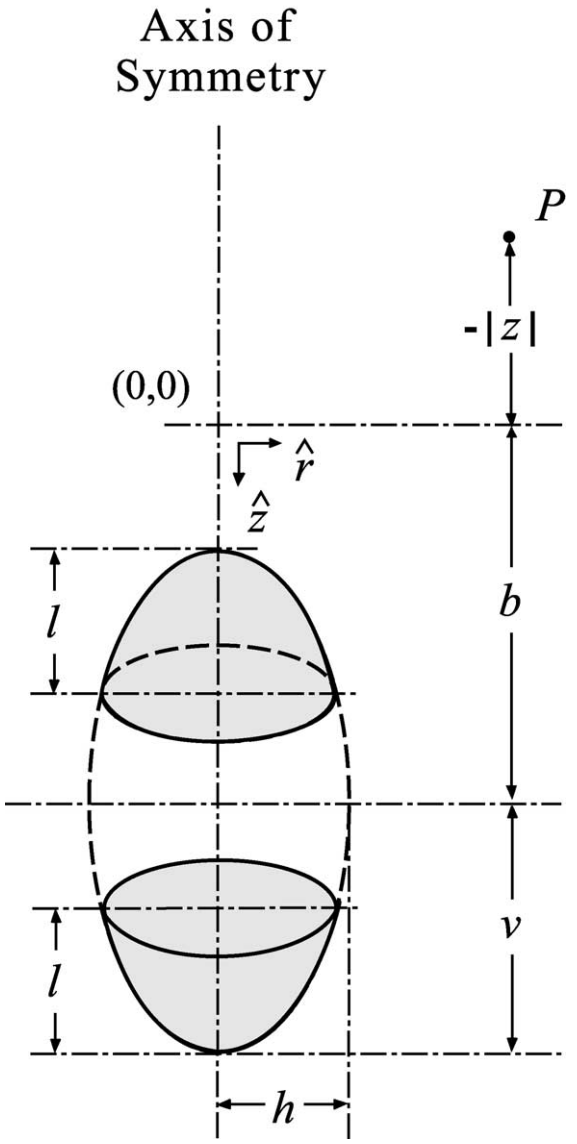

Fig. A9. Schematic diagram for prolate and inverted prolate spheroidal caps.

P at apex of extrapolated cone ($b-z=0$, $\rho'[r']=\rho=$constant).

$$g_z[0,z]=2\pi G\rho\left\{l-\left[\sqrt{a_b^2+(c+l)^2}-\sqrt{a_t^2+c^2}\right]\cos\alpha\right\} \tag{A16}$$

A.4. Inverted right circular cone

P along vertical axis ($r=0$, $\rho'[r']=\rho=$constant).

$$g_z[0,z]=2\pi G\rho\left\{l-\left[(b-z+l)-\overline{A}\right]\cos^2\alpha \pm(b-z+l)\sin^2\alpha\cos\alpha \times\ln\left[\frac{\overline{A}\mp\sqrt{a_t^2+l^2}\pm(b-z+l)\cos\alpha}{(b-z+l)(1\pm\cos\alpha)}\right]\right\} \tag{A17}$$

$$g_z[0,z]=2\pi G\rho\left\{l-\left[(b-z+l)-\overline{A}\right]\cos^2\alpha \pm(b-z+l)\sin^2\alpha\cos\alpha \times\ln\left[\frac{(b-z+l)(1\mp\cos\alpha)}{\overline{A}\pm\sqrt{a_t^2+l^2}\mp(b-z+l)\cos\alpha}\right]\right\} \tag{A18}$$

where $\overline{A}=\sqrt{a_t^2+(b-z)^2}$. Duska (1958, Eq. (9)) gives one form of this solution with $\beta=\alpha$, $\rho=a_t$, $c=b-z$, $d=b-z+l$, $H=\sqrt{a_t^2+l^2}$ and $r_w=\sqrt{a_t^2+(b-z+l)^2}$.

P at centerpoint of base ($r=0$, $b-z=0$, $\rho'[r']=\rho=$constant).

$$\begin{aligned}g_z[0,z]&=2\pi G\rho\sin\alpha\cos\alpha\left\{a_t+l\pm a_t\cos\alpha \times\ln\left[\frac{\cos\alpha(1\mp\cos\alpha)}{\sin\alpha(1\pm\sin\alpha)}\right]\right\}\\&=2\pi G\rho\left(\frac{a_t l}{a_t^2+l^2}\right)\left\{a_t+l\pm\frac{a_t l}{\sqrt{a_t^2+l^2}} \times\ln\left[\frac{l(\sqrt{a^2+l^2}\mp l)}{a(\sqrt{a^2+l^2}\pm a)}\right]\right\}\end{aligned} \tag{A19}$$

A.5. Inverted frustum

P along vertical axis ($r=0$, $\rho'[r']=\rho=$constant).

$$\begin{aligned}g_z[0,z]&=2\pi G\rho\left\{l-(\overline{A}-\overline{B})\cos\alpha \pm(b-z+c+l)\sin^2\alpha\cos\alpha \times\ln\left[\frac{\overline{A}\cos\alpha\mp(b-z+l)\pm(b-z+c+l)\sin^2\alpha}{\overline{B}\cos\alpha\mp(b-z)\pm(b-z+c+l)\sin^2\alpha}\right]\right\}\end{aligned} \tag{A20}$$

$$g_z[0,z] = 2\pi G\rho\left\{ l - (\overline{A}-\overline{B})\cos\alpha \pm (b-z+c+l)\sin^2\alpha\cos\alpha \times \ln\left[\frac{\overline{B}\cos\alpha \pm (b-z)\mp(b-z+c+l)\sin^2\alpha}{\overline{A}\cos\alpha \pm (b-z+l)\mp(b-z+c+l)\sin^2\alpha}\right]\right\} \quad \text{(A21)}$$

where $\overline{A} = \sqrt{a_b^2 + (b-z+l)^2}$ and $\overline{B} = \sqrt{a_t^2 + (b-z)^2}$. Duska (1958, Eq. (10)) gives one form of this solution with $\beta=\alpha$, $\rho_u=a_t$, $\rho_l=a_b$, $a=l$, $c=b-z$, $d=b-z+c+l$, $r_u=\overline{B}$ and $r_l=\overline{A}$.

A.6. Spherical cap

P along vertical axis ($r=0$, $\rho'[r']=\rho=$constant).

$$g_z[0,z] = \frac{2\pi G\rho}{3(b-z)^2}\left\{ a_s^3 - 3(a_s-l)(b-z)^2 + 2(b-z)^3 + \left[a_s^2 + (a_s-l)(b-z) - 2(b-z)^2\right]\sqrt{(b-z-a_s)^2 + 2l(b-z)}\right\} \quad \text{(A22)}$$

$$g_z[0,z] = \frac{4}{3}\pi G\rho l \times \left\{ \frac{2a_s + b - z - \sqrt{(b-z-a_s)^2 + 2l(b-z)}}{\left[b-z-a_s+\sqrt{(b-z-a_s)^2+2l(b-z)}\right]^2}\right\} \quad \text{(A23)}$$

(Duska, 1958, Eq. (13))

P at vertex ($r=0$, $b-z=a_s$, $\rho'[r']=\rho=$constant).

$$g_z[0,z] = 2\pi G\rho l\left\{1 - \frac{1}{3}\sqrt{\frac{2l}{a_s}}\right\} \quad \text{(A24)}$$

P at vertex of half sphere ($r=0$, $l=a_s$, $\rho'[r']=\rho=$constant).

$$g_z[0,z] = 2\pi G\rho a_s\left\{1 - \frac{\sqrt{2}}{3}\right\} \quad \text{(A25)}$$

P along vertical axis of cylinder with spherical cap ($r=0$, $\rho'[r']=\rho=$constant).

$$g_z[0,z] = \frac{2\pi G\rho}{3(b-z)^2}\left\{ a_s^3 + 3(b-z)^2\left(c - z - \sqrt{2a_s l - l^2 + (c-z)^2}\right) - (b-z)^3 + \sqrt{(b-z-a_s)^2 + 2l(b-z)} \times \left[a_s^2 + (a_s-l)(b-z) + (b-z)^2\right]\right\} \quad \text{(A26)}$$

where c is vertical distance between origin and bottom of cylinder.

A.7. Inverted spherical cap

P along vertical axis ($r=0$, $\rho'[r']=\rho=$constant).

$$g_z[0,z] = \frac{2\pi G\rho}{3(b-z)^2}\left\{ a_s^3 - 3(a_s-l)(b-z)^2 - 2(b-z)^3 - \left[a_s^2 - (a_s-l)(b-z) - 2(b-z)^2\right]\sqrt{(b-z+a_s)^2 - 2l(b-z)}\right\} \quad \text{(A27)}$$

$$g_z[0,z] = \frac{4}{3}\pi G\rho l^2 \times \left\{ \frac{2a_s - (b-z) + \sqrt{(b-z+a_s)^2 - 2l(b-z)}}{\left[b-z+a_s\sqrt{(b-z+a_s)^2-2l(b-z)}\right]^2}\right\} \quad \text{(A28)}$$

(Duska, 1958, Eq. (15))

P at centerpoint of base of inverted cap ($r=0$, $b-z=l-a_s$, $\rho'[r']=\rho=$constant).

$$g_z[0,z] = \frac{2\pi G\rho}{3(a_s-l)^2} \times \left\{ a_s^3 - (a_s-l)^3 - (2a_s l - l^2)^{3/2}\right\} \quad \text{(A29)}$$

MacMillan (1958, #6, p. 22) with $x=a_s-l$.

P at centerpoint of inverted half sphere ($r=0$, $b-z=0$, $l=a_s$, $\rho'[r']=\rho=$constant).

$$g_z[0,\,z] = \pi G\rho a_s \tag{A30}$$

A.8. Oblate spheroid

P along vertical axis ($r=0$, $h>v$, $\rho'[r']=\rho=$ constant).

$$g_z[0,\,z] = 4\pi G\rho\left(\frac{h^2 v}{h^2-v^2}\right) \times\left\{1-\frac{b-z}{\sqrt{h^2-v^2}}\tan^{-1}\left[\frac{\sqrt{h^2-v^2}}{b-z}\right]\right\} \tag{A31}$$

MacMillan (1958, p. 18) with $a=h$, $c=v$, $z=(b-z)$, $k^2=G$, $\sigma=\rho$ and change of sign.

A.9. Oblate spheroidal cap

P along vertical axis ($r=0$, $h>v$, $\rho'[r']=\rho=$ constant).

$$g_z[0,\,z] = 2\pi G\rho\left\{l-(v-(b-z)+\overline{A}) \times\left(1-\frac{h^2}{h^2-v^2}\right)-\frac{vh^2(b-z)}{(h^2-v^2)^{3/2}} \times\left(\sin^{-1}\left[\frac{v^2-h^2-lv+\frac{h^2 l}{v}-v(b-z)}{h\sqrt{h^2-v^2+(b-z)^2}}\right] -\sin^{-1}\left[\frac{v^2-h^2-v(b-z)}{h\sqrt{h^2-v^2+(b-z)^2}}\right]\right)\right\} \tag{A32}$$

where $\overline{A}=\sqrt{\frac{h^2}{v^2}(2vl-l^2)+(b-z+l-v)^2}$.

A.10. Inverted oblate spheroidal cap

P along vertical axis ($r=0$, $h>v$, $\rho'[r']=\rho=$ constant).

$$g_z[0,\,z] = 2\pi G\rho\left\{l-(v+(b-z)-\overline{A}) \times\left(1-\frac{h^2}{h^2-v^2}\right)-\frac{vh^2(b-z)}{(h^2-v^2)^{3/2}} \times\left(\sin^{-1}\left[\frac{v^2-h^2-lv+\frac{h^2 l}{v}+v(b-z)}{h\sqrt{h^2-v^2+(b-z)^2}}\right] -\sin^{-1}\left[\frac{v^2-h^2+v(b-z)}{h\sqrt{h^2-v^2+(b-z)^2}}\right]\right)\right\} \tag{A33}$$

where $\overline{A}=\sqrt{\frac{h^2}{v^2}(2vl-l^2)+(b-z+l-v)^2}$.

A.11. Prolate spheroid

P along vertical axis ($r=0$, $v>h$, $\rho'[r']=\rho=$ constant).

$$g_z[0,\,z] = 4\pi G\rho\left(\frac{vh^2}{v^2-h^2}\right)\left\{\frac{b-z}{2\sqrt{v^2-h^2}} \times\ln\left[\frac{b-z+\sqrt{v^2-h^2}}{b-z-\sqrt{v^2-h^2}}\right]-1\right\} \tag{A34}$$

$$g_z[0,\,z] = 4\pi G\rho\left(\frac{vh^2}{v^2-h^2}\right) \times\left\{\frac{b-z}{\sqrt{v^2-h^2}}\tanh^{-1}\left[\frac{\sqrt{v^2-h^2}}{b-z}\right]-1\right\} \tag{A35}$$

A.12. Prolate spheroidal cap

P along vertical axis ($r=0$, $v>h$, $\rho'[r']=\rho=$ constant).

$$g_z[0,z]=2\pi G\rho\left\{l-(v-(b-z)+\overline{A})\times\left(1+\frac{h^2}{v^2-h^2}\right)+\frac{vh^2(b-z)}{(v^2-h^2)^{3/2}}\times\ln\left[\frac{b-z-v+\sqrt{v^2-h^2}-\dfrac{v(b-z)}{\sqrt{v^2-h^2}}}{\overline{A}+\sqrt{v^2-h^2}\left(1-\dfrac{l}{v}\right)-\dfrac{v(b-z)}{\sqrt{v^2-h^2}}}\right]\right\} \tag{A36}$$

where $\overline{A}=\sqrt{\frac{h^2}{v^2}(2vl-l^2)+(b-z+l-v)^2}$.

A.13. Inverted prolate spheroidal cap

P along vertical axis ($r=0$, $v>h$, $\rho'[r']=\rho=$ constant).

$$g_z[0,z]=2\pi G\rho\left\{1-(v+(b-z)-\overline{A})\times\left(1+\frac{h^2}{v^2-h^2}\right)+\frac{vh^2(b-z)}{(v^2-h^2)^{3/2}}\times\ln\left[\frac{b-z+v+\sqrt{v^2-h^2}+\dfrac{v(b-z)}{\sqrt{v^2-h^2}}}{\overline{A}+\sqrt{v^2-h^2}\left(1-\dfrac{l}{v}\right)+\dfrac{v(b-z)}{\sqrt{v^2-h^2}}}\right]\right\} \tag{A37}$$

where $\overline{A}=\sqrt{\frac{h^2}{v^2}(2vl-l^2)+(b-z+l-v)^2}$.

Appendix B. Radial component of gravitational attraction due to vertical, semi-infinite, circular cylinder and horizontal circular disk of infinitesimal thickness

The gravitational potential at $[r, z]$ of a semi-infinite cylinder with constant density is (Singh, 1977, Eq. (4) with $l=\infty$ and change in sign)

$$U[r,z;\ \zeta]=-2\pi G\rho a\int_0^\infty\frac{J_1[a\eta]J_0[r\eta]e^{-\eta(\zeta-z)}}{\eta^2}d\eta \tag{B1}$$

where $J_\mu[x]$ is the Bessel function of order μ and argument x and other variables as previously defined. Noting that

$$J_0'[r\eta]=-\eta J_1[r\eta],$$

the radial component of gravitational attraction has the form

$$g_r[r,z;\ \zeta]=-\frac{\partial U}{\partial r}=-2\pi G\rho a\int_0^\infty\frac{J_1[a\eta]J_1[r\eta]e^{-\eta(\zeta-z)}}{\eta}\mathrm{d}\eta. \tag{B2}$$

This integral is of the Lipschitz–Hankel type and has been evaluated by Eason et al. (1955, Eq. (4.9)). The resulting closed-form solutions are

$$g_r[r,z;\ \zeta]_{r<a}=-\frac{G\rho}{r}\left\{\pi r^2+(\zeta-z)\sqrt{(a+r)^2+(\zeta-z)^2}\times E[k_1]-(\zeta-z)\frac{(2a^2+2r^2+(\zeta-z)^2)}{\sqrt{(a+r)^2+(\zeta-z)^2}}K[k_1]+\frac{\pi}{2}(a^2-r^2)\Lambda_0[\phi,k_1]\right\} \tag{B3a}$$

$$g_r[r, z; \zeta]_{r=a} = -\frac{G\rho}{a}\left\{\pi a^2 + (\zeta - z)\sqrt{4a^2 + (\zeta - z)^2}E[k_1] - (\zeta - z)\frac{(4a^2 + (\zeta - z)^2)}{\sqrt{4a^2 + (\zeta - z)^2}}K[k_1]\right\} \quad \text{(B3b)}$$

$$g_r[r, z; \zeta]_{r>a} = -\frac{G\rho}{r}\left\{\pi a^2 + (\zeta - z)\sqrt{(a + r)^2 + (\zeta - z)^2} \times E[k_1] - (\zeta - z)\frac{(2a^2 + 2r^2 + (\zeta - z)^2)}{\sqrt{(a + r)^2 + (\zeta - z)^2}} \times K[k_1] + \frac{\pi}{2}(r^2 - a^2)\Lambda_0[\phi, k_1]\right\}. \quad \text{(B3c)}$$

Along the top of a semi-infinite cylinder (i.e., $z = \zeta$) with constant density, Eqs. (B3a–3c) reduce to

$$g_r[r, z; \zeta]_{r<a} = -\pi G\rho r \quad \text{(B4a)}$$

$$g_r[r, z; \zeta]_{r=a} = -\pi G\rho a \quad \text{(B4b)}$$

$$g_r[r, z; \zeta]_{r>a} = -\pi G\rho\left(\frac{a^2}{r}\right). \quad \text{(B4c)}$$

The radial component of gravitational attraction caused by a vertical, semi-infinite, circular cylindrical shell can be obtained from Eq. (B2) by superimposing two semi-infinite cylinders with slightly different radii Δa and then shrinking this difference to zero. In this case, the volume–mass density, ρ, is replaced with a surface-mass density, σ, such that $\sigma = \rho\Delta a$ but remains nonzero as $\Delta a \to 0$. Taking the derivative of Eq. (B2) with respect to a yields

$$g_r^{\text{shell}}[r, z] = \frac{\partial}{\partial a}g_r[r, z; \zeta]\Delta a = -2\pi G\sigma a\int_0^\infty J_0[a\eta]J_1[r\eta]e^{-\eta(\zeta - z)}\mathrm{d}\eta. \quad \text{(B5)}$$

This integral has the closed-form solutions (Eason et al., 1955, Eq. (4.7))

$$g_r^{\text{shell}}[r, z; \zeta]_{r<a} = -2G\sigma\left(\frac{a}{r}\right)\left\{-\frac{(\zeta - z)}{\sqrt{(a + r)^2 + (\zeta - z)^2}}K[k_1] + \frac{\pi}{2}\Lambda_0[\phi, k_1]\right\} \quad \text{(B6a)}$$

$$g_r^{\text{shell}}[r, z; \zeta]_{r=a} = -2G\sigma\left\{\frac{\pi}{2} - \frac{(\zeta - z)}{\sqrt{4a^2 + (\zeta - z)^2}} \times K\left[\frac{2a}{\sqrt{4a^2 + (\zeta - z)^2}}\right]\right\} \quad \text{(B6b)}$$

$$g_r^{\text{shell}}[r, z; \zeta]_{r>a} = -2G\sigma\left(\frac{a}{r}\right)\left\{\pi - \frac{(\zeta - z)}{\sqrt{(a + r)^2 + (\zeta - z)^2}}K[k_1] + \frac{\pi}{2}\Lambda_0[\phi, k_1]\right\}. \quad \text{(B6c)}$$

The radial component of gravitational attraction caused by a horizontal circular disk of infinitesimal thickness is obtained from Eq. (B2) by superimposing two semi-infinite cylinders separated by the vertical distance $\Delta\zeta$ and then shrinking this distance to zero. For this case, the volume–mass density is replaced with a surface-mass density such that $\sigma = \rho\Delta\zeta$ but

remains nonzero as $\Delta\zeta \to 0$. Taking the derivative of Eq. (B2) with respect to ζ yields (see Eason et al., 1955, Eq. (4.2))

$$g_r^{\text{disk}}[r, z] = -\frac{\partial}{\partial\zeta} g_r[r, z; \zeta]\Delta\zeta$$
$$= -2\pi G\sigma a \int_0^\infty J_1[a\eta]J_1[r\eta]e^{-\eta(\zeta-z)}\mathrm{d}\eta$$
$$= -\frac{2G\sigma}{r}\sqrt{(a+r)^2+(\zeta-z)^2}$$
$$\times\left\{\left(1-\frac{k_1^2}{2}\right)K[k_1]-E[k_1]\right\}. \qquad \text{(B7)}$$

References

Beaumont, C., 1978. The evolution of sedimentary basins on a viscoelastic lithosphere: theory and examples. Geophysical Journal of the Royal Astronomical Society 55, 471–497.

Bodine, J.H., Karner, G.D., 1981. Gravity effect of axially symmetric bodies using the one-dimensional FFT. Geophysical Journal of the Royal Astronomical Society 67, 747–754.

Brotchie, J.F., 1971. Flexure of a liquid-filled spherical shell in a radial gravity field. Modern Geology 3, 15–23.

Byrd, P.F., Friedman, M.D., 1954. Handbook of Elliptic Integrals for Engineers and Physicists. Springer-Verlag.

Damiata, B.N., Lee, T.-C., 2002. Gravitational attraction of solids of revolution: Part 1. Vertical circular cylinder with radial variation of density. Journal of Applied Geophysics, this issue.

Duska, L., 1958. Maximum gravity effect of certain solids of revolution. Geophysics 23, 506–519.

Eason, G., Noble, B., Sneldon, I.N., 1955. On certain integrals of Lipschitz–Hankel type involving products of Bessel Functions. Philosophical Transactions of the Royal Astronomical Society of London, Series A 247, 529–551.

Garland, G.D., 1951. Combined analysis of gravity and magnetic anomalies. Geophysics 16, 51–62.

Götze, H.-J., Lahmeyer, B., 1988. Application of three-dimensional interactive modeling in gravity and magnetics. Geophysics 53, 1096–1108.

Grant, F.S., West, G.F., 1965. Interpretation Theory in Applied Geophysics. McGraw-Hill.

MacMillan, W.D., 1958. The Theory of the Potential. Dover Publications.

McNutt, M., Menard, H.W., 1978. Lithospheric flexure and uplifted atolls. Journal of Geophysical Research 83, 1206–1212.

Nabighian, M.N., 1962. The gravitational attraction of a right vertical circular cylinder at points external to it. Geofisica Pura e Applicata 53, 45–51.

Pant, M.M., Govindarajan, J., 1979. Computation of gravity effects of two- and three-dimensional bodies with radial symmetry. Computers and Geosciences 5, 313–323.

Paul, M.K., 1985. Approximate computation of radial gravity profiles for sources with circular symmetry. Geophysics 50, 1307–1310.

Piessens, R., de Doncker-Kapenga, E., Überhuber, C.W., Kahaner, D.K., 1983. QUADPACK: A Subroutine Package for Automatic Integration. Springer-Verlag.

Pohánka, V., 1988. Optimum expression for computation of the gravity field of a homogeneous polyhedral body. Geophysical Prospecting 36, 733–751.

Press, W.H., Teukolsky, S.A., Vetterling, W.T., Flannery, B.P., 1992. Numerical Recipes. Cambridge Univ. Press.

Reilly, W.I., 1969. Gravitational and magnetic effects of a right circular cylinder. New Zealand Journal of Geology and Geophysics 12, 497–506.

Reilly, W.I., 1972. Gravitational expression of the Dunedin volcano. New Zealand Journal of Geology and Geophysics 15, 16–21.

Robertson, E.I., 1967a. Gravity effects of volcanic islands. New Zealand Journal of Geology and Geophysics 10, 1466–1483.

Robertson, E.I., 1967b. Gravity survey in the Cook Islands. New Zealand Journal of Geology and Geophysics 10, 1484–1498.

Robertson, E.I., Kibblewhite, A.C., 1966. Bathymetry around isolated volcanic islands and atolls in the South Pacific Ocean. New Zealand Journal of Geology and Geophysics 9, 111–121.

Shampine, L.F., Allen Jr., R.C. 1973. Numerical Computing: An Introduction. Saunders.

Singh, S.K., 1977. Gravitational attraction of a vertical right circular cylinder. Geophysical Journal of the Royal Astronomical Society 50, 243–246.

Singh, S.K., Sabina, F.J., 1978. Magnetic anomaly due to a vertical right circular cylinder with arbitrary polarization. Geophysics 43, 173–178.

Singh, S.K., Castro, E.R., Guzman, S.M., 1979. Magnetic anomaly of a circular lamina. Geophysics 44, 102–107.

Talwani, M., 1973. Computer usage in the computation of gravity anomalies. Methods in Computational Physics: Advances in Research and Applications, vol. 13. Academic Press, pp. 343–389.

Woodward, D.J., 1970. Gravity and magnetic anomalies over the Derwent–Hunter guyot, Tasman sea. New Zealand Journal of Geology and Geophysics 13, 117–125.

Woodward, D.J., 1973. Gravitational and magnetic effects of a solid of revolution. New Zealand Journal of Geology and Geophysics 16, 170–171.

Zwillinger, D., 1992. Handbook of Integration. Jones and Bartlett Publishers.